Lab on a Chip

RSC Publishing

PAPER

View Article Online
View Journal | View Issue

Electrokinetic tweezing: three-dimensional manipulation of microparticles by real-time imaging and flow control†

Cite this: *Lab Chip*, 2013, **13**, 4040

Zachary Cummins,*[a] Roland Probst[b] and Benjamin Shapiro[ac]

Received 3rd June 2013,
Accepted 19th July 2013

DOI: 10.1039/c3lc50674f

www.rsc.org/loc

Electrokinetic tweezing in three dimensions is achieved for the first time using a multi-layer microfluidic device, a model-based control algorithm, and a 3D imaging algorithm connected in a feedback loop. Here we demonstrate steering of microparticles along 3D trajectories and trapping in all three dimensions with accuracy as good as 1 μm.

Introduction

Vision-based electrokinetic feedback control has allowed simple microfluidic devices to manipulate microscopic[1–3] and nanoscopic[4–7] objects on chip, and has advantages over other methods. Electrokinetic (EK) tweezing, which uses electrophoretic (EP)[8] forces and/or electroosmotic (EO)[9,10] flows, allows control of the position of essentially any visible object which acquires an electric surface charge, or that is suspended in a fluid that exhibits EO flow, or both.[11] It has allowed the manipulation of one and multiple cells,[3,11] single protein molecules and fluorophores,[12] and nanoscopic quantum dots.[6,7,13] EK tweezers require less actuation effort than other methods to manipulate nanoscopic particles due to the favorable scaling of EO actuation with particle size (drag forces scale with the radius of the particle[14] rather than with its volume as do optical,[15] dielectrophoretic,[16] and magnetic forces[17]). This favorable scaling has enabled EO manipulation and trapping of single quantum dots to tens of nanometers precision[6] – the best reported precision of any method to date. EK manipulation has also been used to control the orientation of nanorods in addition to their positions by modulating the shear forces around them.[18,19]

However, all of these prior EK results have been restricted to two spatial dimensions. Here, we present a device design, associated physical modeling, 3D imaging, feedback control, and experimental results for 3-dimensional EK tweezing. As in previous work,[20–22] EK actuation in the third dimension (3D) is enabled by a multi-layer device. The device is fabricated by cutting microchannels into several films of polydimethylsiloxane (PDMS) and stacking them one on top of the other to form a control volume at their intersection. When voltages are applied from one layer to another, the created electric fields (for EP actuation) or fluid flows (for EO actuation) have a vertical component. Exploitation of this vertical component enables control of single particles in all 3 dimensions.

We first briefly summarize how EK tweezers work in two spatial dimensions before showing how to extend the method to work in the third dimension. As shown in Fig. 1, for a 2D microfluidic device, a control algorithm, and a particle tracking system (microscope, camera, and software) are connected in a real-time feedback loop. At each time step, the particle tracking system measures the position of a chosen particle. The control algorithm then compares this measured position with the particle's desired position and calculates the necessary voltages to create an EK velocity to move that particle from where it is towards where it should be. This feedback loop repeats continually, and at each time moves the chosen particle toward its desired position, thus either trapping it at a stationary target, or steering it along a complex trajectory by dynamically updating the target.[1–3,7,11] This process is robust to imperfections in the microfluidic device and modeling uncertainties: so long as the control algorithm knows how to move the particle from where it is *towards* where it should be, the positioning error is decreased at each time step, and the particle quickly reaches its target location – and it does so with nanoscale precision if the system has been optimized.[6,7]

Materials and methods

Design and fabrication of a multi-layer 3D microfluidic control device

In this paper, the horizontal and vertical forces needed for 3D manipulation are produced with a microfluidic device that

[a]*Fischell Department of Bioengineering, University of Maryland, College Park, MD, 20742, USA. E-mail: zcummins@umd.edu*
[b]*ACUITYnano, LLC, Rockville, MD, 20850, USA*
[c]*Institute for Systems Research, University of Maryland, College Park, MD, 20742, USA*

† Electronic supplementary information (ESI) available. See DOI: 10.1039/c3lc50674f

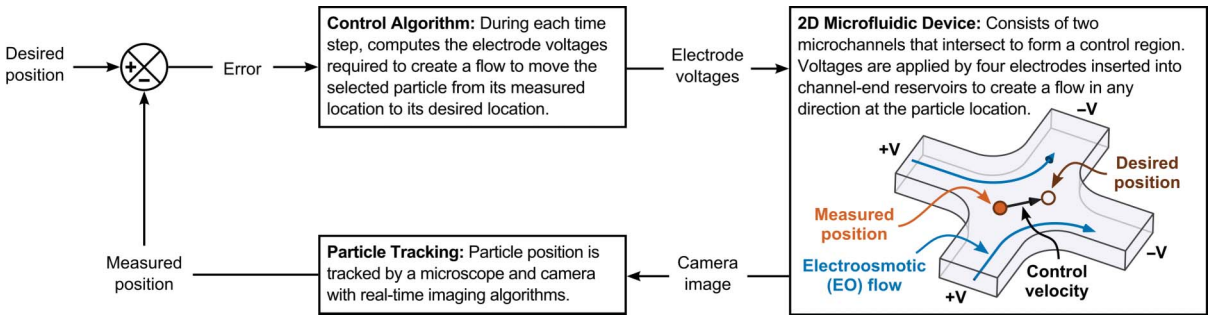

Fig. 1 Schematic of vision-based electrokinetic feedback control in two dimensions. The system is shown manipulating a neutral particle with electroosmotic (EO) flow only. A microfluidic device, control algorithm, and particle tracking system are connected in a real-time feedback loop. The vision tracking system measures the position of a particle chosen by a user. The control algorithm then calculates which EO fluid flow will carry this particle from its current towards its desired position, and electrodes then actuate the necessary fluid flow. This feedback loop repeats continually and at each time moves the chosen particle closer to its desired position, thus either trapping it in place or steering it along any desired trajectory.

consists of five layers of PDMS microchannels stacked on a microscope slide. PDMS films of 250 μm thickness were patterned with microchannels using a desktop vinyl cutter (Lynx 12, Sign Warehouse, Denison, TX, USA). As shown in Fig. 2(a), each PDMS layer possesses eight circular reservoirs of 3 mm diameter spaced equally around a 15 mm diameter radial pattern. The bottom four layers also possess a single straight microchannel that extends between the left-most and right-most reservoirs and chokes to a width of 385 μm at its midpoint. The layers were stacked and aligned by hand on a microscope, beginning by placing the first microchannel layer on a glass microscope slide. The remaining microchannel layers were rotated 45, 90, and 135 degrees clockwise (from the bottom to the top) relative to the first layer before being aligned and stacked on the layer below. The fifth and final layer only possesses holes for the eight channel-end reservoirs, and seals the top microchannel. The four microchannels intersect at the center of the completed device to form an octagonal column in which particles entering from a microchannel at the top can move into a microchannel at the bottom, and *vice versa*.

Electrodes inserted into the eight channel-end reservoirs (two for each of the four channels) create an electric field in the microfluidic device that produces 3D EP and EO actuation. As shown in Fig. 2(b), when a positive potential is applied to an electrode in the top microchannel and a negative potential is applied to an electrode in the bottom microchannel, both the EP (orange dash) and EO (blue dot-dash) effects produce vertical velocities in the control volume. Any particle in the control volume can therefore experience a sinking or lifting force if actuation is applied from a top electrode to one below it, or *vice versa*. By properly actuating each of the eight electrodes at once we are able to precisely control both the horizontal and vertical velocities of any chosen particle. The vertical EK velocities used to steer a particle along the ∞ trajectory shown in Fig. 2(b) are shown in Fig. S1 of the ESI.†

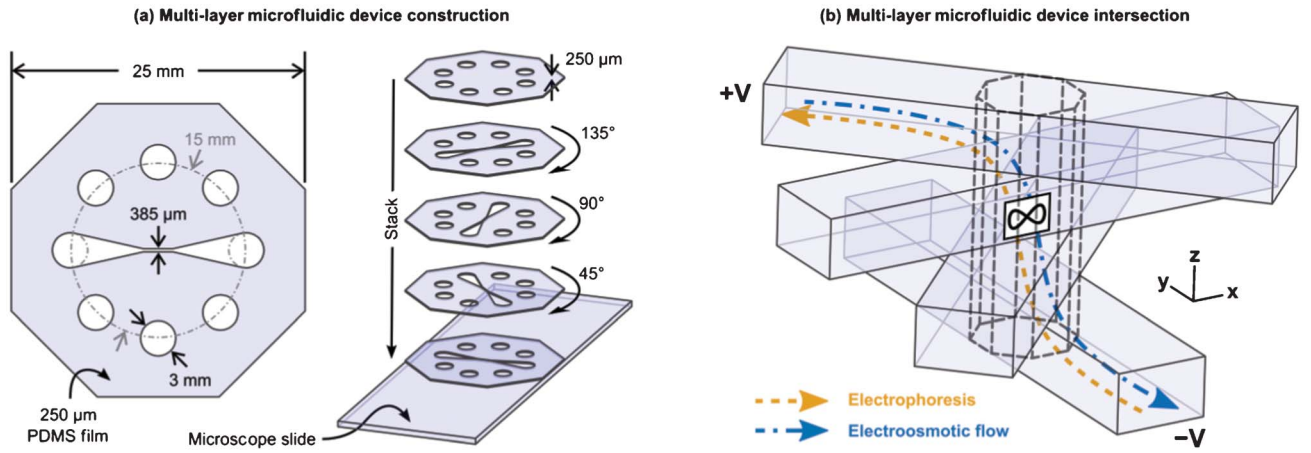

Fig. 2 Design, fabrication, and modeling of the multi-layer microfluidic control device. (a) Four layers of PDMS film of 250 mm thickness were patterned to have a single microchannel and were stacked and aligned to form an octagonal control volume at the center of the device. A fifth layer, without microchannels, sealed the device. (b) When this device is actuated from top left (+V voltage) to bottom right (−V voltage), an EO flow is created from top left to bottom right (blue arrow) that drags all particles present in the device. A particle which possesses a surface charge will also experience an EP velocity in addition to the EO flow. For example, a particle with a negative surface charge will experience an EP velocity (orange arrow) which opposes the EO velocity.

The horizontal components of the EK velocity are similar to those in our prior 2-dimensional EK tweezing devices.[3,23]

Modeling and simulation of electrokinetic forces

To design the 3D control algorithm, we must first predict the 3-dimensional EO flows and EP force fields that will be created by voltage actuations. In EP actuation, a particle with surface charge moves under the influence of the 3D electric field created when a voltage is applied across the eight channel-end electrodes. The EP velocity $\vec{v}_{EP}$ of a charged particle in a quiescent fluid is given by the Helmholtz–Smoluchowski relation:[24]

$$\vec{v}_{EP}(x,y,z) = \mu_{EP}\,\vec{E}(x,y,z) = \frac{\varepsilon_r \varepsilon_0 \zeta_p}{\eta}\vec{E}(x,y,z), \quad (1)$$

where μ_{EP} is the EP mobility of the particle, ζ_P is the zeta potential of the particle, η is the dynamic viscosity of the liquid, ε_0 is the dielectric constant in vacuum, and ε_r is the relative dielectric constant of the liquid. The electric field $\overrightarrow{E} = -\nabla\Phi$ is described by Laplace's equation subject to boundary conditions set by the potentials applied at the eight electrodes.[25]

In EO actuation, an electric double layer forms at the interface between the walls of the microchannel and the electrolyte medium, this double layer moves under the influence of the electric field and drags the adjacent fluid and particles by viscous forces.[24] We therefore compute the EO fluid velocities by solving the low-Reynolds number fluid equations (Stokes equations) with the moving double layer as boundary conditions,[26,24] and we find that the directions of the 3D EO flows in our device are almost along the electric field. For a negatively charged particle, this means the EO velocities basically point opposite to the EP velocities at every location in the device (compare the yellow and blue arrows in Fig. S1 of the ESI†). We therefore estimate the EO velocity to be

$$\vec{v}_{EO} = \mu_{EO}\,\vec{E} \quad (2)$$

where μ_{EO} is the EO mobility of the device. Combining eqn (1) and (2), the EK velocity of a particle in the device is thus given by

$$\vec{v}_{EK} = \mu_{EP}\,\vec{E} + \mu_{EO}\,\vec{E} = \mu_{EK}\,\vec{E} \quad (3)$$

where $\mu_{EK} = \mu_{EP} + \mu_{EO}$ is the net EK mobility of a particle in the microfluidic device, and μ_{EP} is positive (or negative) if the particle is positively (or negatively) charged.

Feedback control algorithm

Control design for 3D manipulation is similar to our previously published 3D control simulations.[22] Briefly, we calculate a map from the electric potentials applied to the eight channel-end electrodes to the resulting motion of a particle at any location in the device. Since Laplace's equation for the electric field is linear, we can rewrite eqn (3) for the EK velocity as a superposition of the velocities produced by each electrode alone

$$\begin{aligned}\vec{v}_{EK}(x,y,z,t) &= \sum_{i=1}^{8} \vec{v}_{EK,i}(x,y,z)\,V_i(t) \\ &= A(x,y,z)\,\vec{V}(t),\end{aligned} \quad (4)$$

where $\vec{v}_{EK,i}$ is the 3D EK velocity of a particle when a unit potential is applied to electrode i with all other electrodes set to zero, and V_i is the instantaneous potential applied to electrode i during control. The matrix $A = [\vec{v}_{EK,1}\ \vec{v}_{EK,2} \ldots \vec{v}_{EK,8}]$ contains the EK velocities created by each electrode alone and $\overrightarrow{V} = [V_1\ V_2\ \ldots\ V_8]^T$ is the vector of all electrode potentials. Eqn (4) is the mapping from the applied voltage $\overrightarrow{V}$ to the resulting velocity $\vec{v}_{EK}$ of any particle. At each time step of the control loop this map, evaluated at the chosen particle's current (x,y,z) location, is inverted to find the voltages that will create an actual velocity as close as possible to the desired particle velocity $\vec{v}_d$. This leads to the control law

$$\vec{V}(t) = kA^*(x,y,z)\,\vec{v}_d(t) \quad (5)$$

where k is a positive scalar gain changed to tune control performance, (x,y,z) is the location of the chosen particle, and $A^* = (A^TA)^{-1}A^T$ is the pseudo-inverse of the linear map (eqn (4)) evaluated at the location of the chosen particle.

For precise control in three dimensions at least four electrodes are required for each controlled particle. Additional electrodes enhance directional control and reduce the effort required from the other electrodes, as discussed in detail by Chaudhary and Shapiro.[23] The eight electrode device presented here can therefore potentially manipulate two particles in three dimensions simultaneously.

3D imaging

For the control algorithm to work, it needs to know the location (x,y,z) of the particle. This location is sensed, in real-time, by a single camera and a defocus imaging method.[27–30] A ''defocus mask'' with multiple apertures is positioned between the infinity-corrected objective lens and the tube lens of a conventional wide-field microscope with video camera, as illustrated in Fig. 3(a) for two apertures. Light from a particle below the focal plane diverges through each aperture and reaches the image sensor of the camera at two separate locations. Conversely, light from an object positioned above the focal plane converges through each aperture, intersects before reaching the image sensor, and reaches the sensor at two separate, but flipped, locations. The distance between the two locations increases as the particle moves vertically away from the focal plane: this allows measurement of the distance of the particle from the focal plane, but does not indicate which side of the focal plane the particle is on.

A defocus mask with three apertures was used to project three images of each particle onto the image sensor in a pattern which scales linearly with the displacement of the particle from the focal plane, as well as flips orientation as the particle crosses the focal plane. The mask, as shown in Fig. 3 (b), consisted of three apertures of 2 mm diameter separated by equal distance around a 4 mm diameter circle. The mask was laser-printed onto a clear transparency film and mounted on the back of the 20× magnification objective lens of a

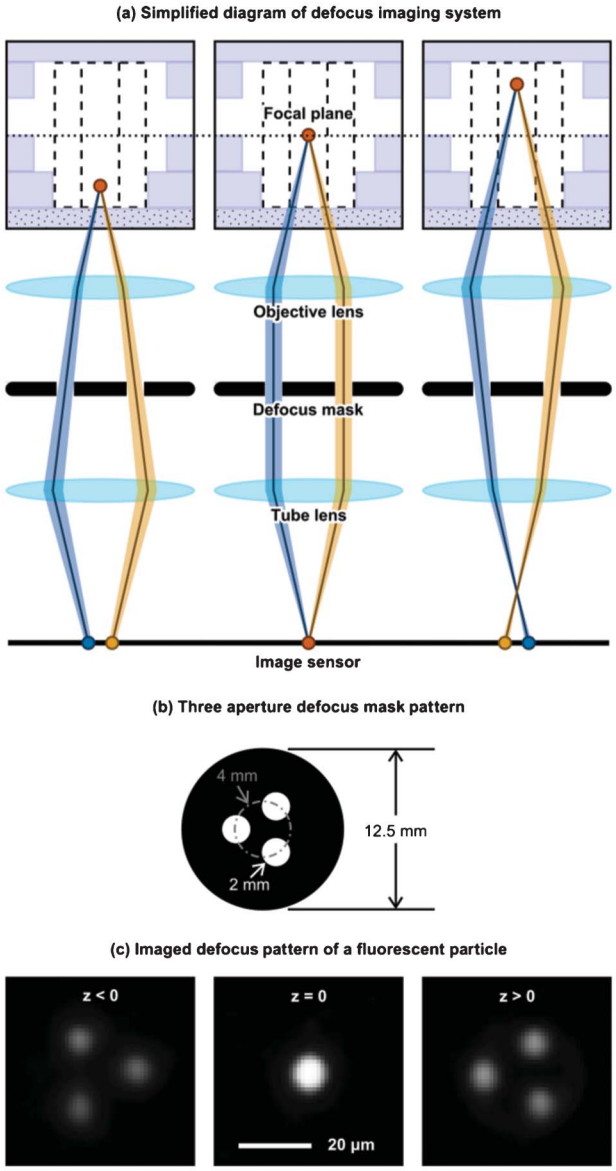

Fig. 3 Single-camera defocus imaging concept.[27–30] In this simplified diagram, light from a particle passes through two apertures printed in a ''defocus mask'' mounted between an infinity-corrected objective lens and the tube lens of the microscope. Light from an object below the focal plane is captured at the image plane in two locations separated by a distance which scales with particle elevation. This image flips as the particle crosses the focal plane while a particle at the focal plane appears in focus. (b) To determine which side of the focal plane a particle is on, a mask with three apertures of 2 mm diameter arranged radially in a 4 mm diameter pattern was mounted on the back of a microscope objective. (c) The three projections of an out-of-focus particle appear at the vertices of an equilateral triangle. The distance between the projections scales with the elevation of the particle, and the orientation of the defocus pattern is flipped depending on which side of the focal plane the particle is on.

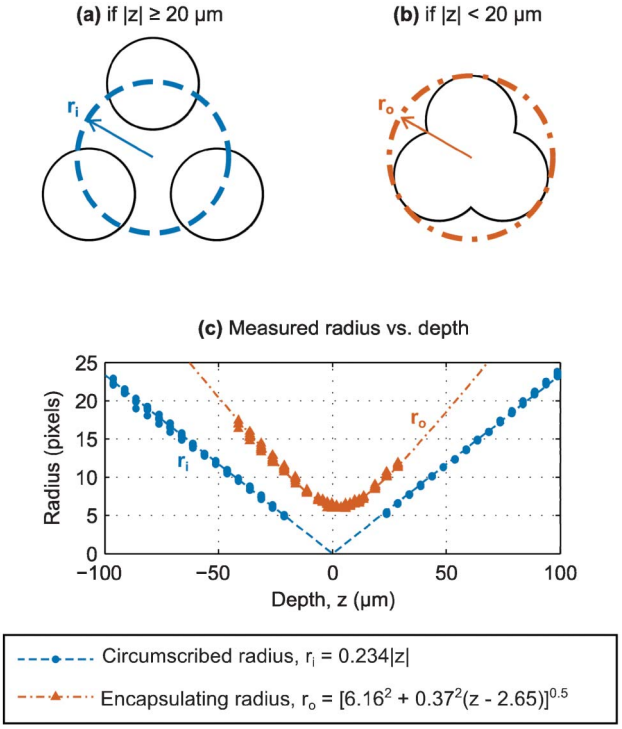

Fig. 4 Defocus pattern image processing. (a) Away from the focal plane ($|z| \geqslant 20$ μm) the three projections of a particle are segregated and appear in the image as individual bright spots. A circle of radius r_i is inscribed through the centroids of the projections. (b) Near the focal plane ($|z| \leqslant 20$ μm) the three projections overlap in the image, requiring an alternate metric of particle elevation. Therefore, a circle of radius r_o is drawn around the extent of the aggregate defocus pattern. (c) The inscribed radius r_i scales linearly with the displacement of a particle from the focal plane at a rate of 0.234 pixels μm^{-1} (blue circles), while the encapsulating radius r_o scales hyperbolically with a semi-major axis of 6.16 pixels and semi-minor axis of 0.37 μm centered around z = 2.65 μm.

microscope. Using this mask as in Fig. 3(c), particles positioned above and below the focal plane are imaged as groups of three bright spots located at the vertices of an equilateral triangle whose orientation is flipped depending on which side of the focal plane the particle is on. Particles at the focal plane (z = 0 μm) appear in focus, with all three projections overlapping.

The vertical position of a particle is determined by measuring the spread of its three projections. In each image acquired from the camera, the projections of every visible particle are found by identifying regions of pixels with intensities above a threshold. A simple algorithm then locates groups of three projections that match the triangular configuration of the defocus mask and circumscribes a circle of radius r_i through each group, as shown in Fig. 4(a). The side of the focal plane a particle is on is easily determined by whether the group matches the orientation of the normal or flipped triangular configuration. However, when a particle is near the focal plane its three projections overlap and must be measured in another way. As shown in Fig. 4(b), the overlapping defocus pattern spread is quantified by fitting a circle of radius r_o around the extent of the three projections. The normal or flipped orientation of the overlapping defocus pattern is more difficult to determine and leads to increased uncertainty in measurements made near the focal plane. As shown in Fig. 4(c), the circle of radius r_i (blue circles) through each projection of the defocus pattern scales linearly with the

elevation of the particle, while the circle of radius r_o (red triangles) drawn around the extent of the overlapping defocus pattern scales hyperbolically. This hyperbolic scaling around the focal plane leads to a higher sensitivity of the imaging algorithm to noise: even a small change in r_o will cause a large change in the inferred particle elevation. We reduce this uncertainty by applying a Kalman filter to the 3D measurement of the position of each tracked particle in real-time.[31] Details of the Kalman filter are included in the ESI.†

In the event that the triangular configurations of multiple particles overlap, the prediction of the Kalman filter is used to select the correct particle. This allows one particle to be steered and trapped in a crowd of many particles.

Experimental setup

Combining the 3D imaging above with our top to bottom electrokinetic actuation enables 3D EK tweezing. The multilayer microfluidic device is observed using an inverted wide-field microscope (TS100, Nikon Corporation, Tokyo, Japan) with 20× fluorescent objective (Plan Fluor, Nikon Corporation, Tokyo, Japan) and a charge-coupled device camera (Guppy F-033C, Allied Vision Technologies, Stadtroda, Germany) that are calibrated for 3D defocus imaging. Eight electrodes are inserted into each of the eight channel-end reservoirs of the device and connected to a digital-to-analog voltage output device (USB-3106, Measurement Computing, Norton, MA, USA) that is in turn connected to a personal computer. Custom software locates, tracks, and manipulates, in real-time, any chosen object in the control volume. During each iteration of the control loop, the desired position of the object is dynamically updated with coordinates supplied either by user input or by a pre-planned trajectory. The voltages required to move the particle from its measured position towards its desired position are calculated by the control algorithm and are applied to the microfluidic device. This loop is continually repeated at ~20 Hz, enabling steering of objects along complex trajectories as well as precise and accurate trapping of objects in 3D.

Results and discussion

3D steering of a single polystyrene microsphere

To demonstrate 3D electrokinetic tweezing, we steered a single polystyrene microsphere of 5 μm diameter (G0500, Duke Scientific Corporation, Palo Alto, CA, USA) along the edges of a tilted cube. Fig. 5(a) shows the two-dimensional images acquired from the camera at four different time points as the microsphere was steered along the desired trajectory with a constant velocity of 2.5 μm s^{-1}. The trajectory of the microsphere (orange dots) closely follows the desired cube trajectory (solid green line). Fig. 5(b) shows a trace of the 3D path of the microsphere. During steering, the increased imaging error near the focal plane is mitigated by a Kalman filter, which uses the EK velocity predicted by the mathematical model to estimate which side of the focal plane the microsphere is on. The errors measured here for 3D steering are comparable to the error attained with our early 2D steering results.[2,3]

3D trapping of a single polystyrene microsphere

To quantify EK trapping accuracy, we trapped microspheres at several elevations in the control volume. Microspheres trapped

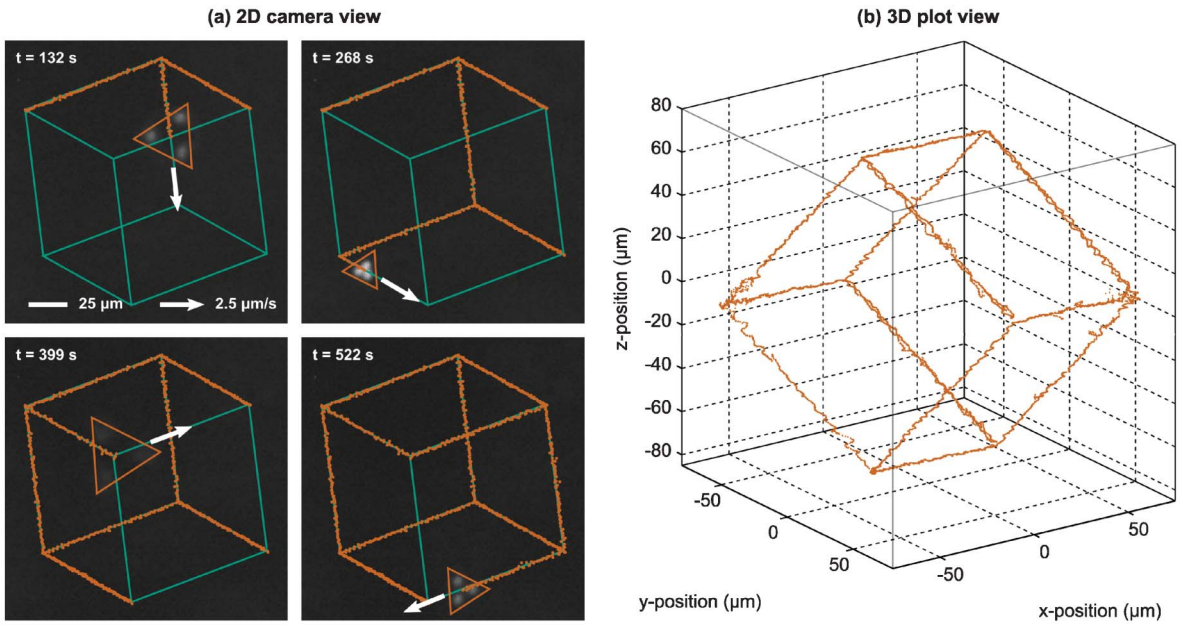

Fig. 5 A single polystyrene microsphere of 5 μm diameter was steered along the edges of a tilted cube at a velocity of 2.5 μm s^{-1}. (a) The camera image modified by the defocus mask is shown at times t = 132, 268, 399, and 522 s. The desired cube trajectory is overlaid as a solid green line and the path taken by microsphere is shown by orange dots. (b) A 3D plot of the complete path taken by the microsphere. The microsphere was steered with an RMS error of 1.17 μm in the xy plane and 1.25 μm in the vertical z direction. A video of this experiment is available as ESI†.

below the focal plane ($z < -20$ μm) were trapped with a root-mean-square (RMS) error of less than 1 μm both in the *xy* plane and in the *z* direction. Microspheres trapped above the focal plane ($z > 20$ μm) experienced the same accuracy in the *xy* plane, but a slightly decreased accuracy in the *z* direction of ~1.5 μm (at this time it is still unclear why trapping accuracy in the *z* direction differs slightly from one side of the focal plane to the other). At the focal plane, microspheres were trapped with an RMS error of ~1.5 μm in the plane and ~2.5 μm in the *z* direction. Increased error in the *z* direction for a microsphere near the focal plane is due to increased imaging sensitivity to noise, as discussed above, as well as errors due to uncertainty in whether the particle is above or below the focal plane.

Accuracy of 3D imaging

The accuracy of the above imaging algorithm was quantified by measuring the elevation of microspheres adhered to a device as the device was raised and lowered by manually adjusting the fine focus of the microscope. Fluorescent polystyrene microspheres of 5 μm diameter were dried in place in the microchannels of a microfluidic device, and the device was raised and lowered from $z = -80$ μm to $z = +80$ μm. The vertical imaging range is limited primarily by the numerical aperture (NA) of the microscope objective lens: as the NA of a lens increases, the vertical depth in which a particle is detectable decreases. In the *xy* horizontal plane, the microspheres were tracked throughout the measured range with a standard deviation as good or better than $\sigma_{xy} \approx 0.1$ μm. In the vertical *z* direction, the standard deviation varied with the distance of the microspheres from the focal plane, and was nearly the same on either side of the focal plane. Microspheres located near the focal plane ($|z| \leqslant 20$ μm), where the three projections of each microsphere overlap, were tracked with a vertical standard deviation of $\sigma_z \approx 0.4$ μm. Microspheres at a distance of $|z| \approx 20$ μm from the focal plane, where the three projections first separate (as in (a) of Fig. 4), were imaged with a vertical standard deviation of approximately $\sigma_z \approx 0.05$ μm, as good as the imaging accuracy in the *xy* horizontal plane. For particle elevations between 20 and 80 μm from the focal plane, the three projections of each microsphere gradually blur and dim, resulting in a gradual degradation of the standard deviation from $\sigma_z \approx 0.05$ μm at $|z| = 20$ μm to $\sigma_z \approx 0.15$ μm at $|z| = 80$ μm.

Conclusions

In summary, we have demonstrated electrokinetic manipulation of microparticles in three dimensions using a novel multi-layer microfluidic device design, a pseudo-inverse model-based control algorithm, and a single-camera defocus imaging system. The multi-layer microfluidic device is fabricated with a desktop fabrication technique and produces both the horizontal and vertical forces necessary for manipulation of particles in all three dimensions. The position of each particle is estimated in real-time using a defocus imaging system that masks out-of-focus particles into a triangular pattern that scales with the elevation of the particle. Using this system we demonstrated steering of polystyrene microspheres of 5 μm diameter along a three-dimensional trajectory, as well as stationary trapping to an accuracy of approximately 1 μm.

EK tweezers have advantages compared to other methods – the systems are relatively inexpensive and applied EO viscous forces scale with particle radius rather than particle volume[24,11] enabling nanoprecise control of nanoscale objects.[13,7] However, to date, EK tweezing has been limited to 2 spatial dimensions. To the best of our knowledge, this is the first experimental demonstration that electrokinetic tweezing can be extended to manipulate single objects in all 3 dimensions.

Acknowledgements

This work was supported in part by DARPA (W31P4Q0810007) and by the National Science Foundation (CAREER grant, program managers Maria Burka and Kishan Baheti, grant number ECS0348251). We also wish to acknowledge K. Saadin for useful discussion.

References

1 M. Armani, S. Chaudhary, R. Probst and B. Shapiro in *μTAS*, Malmo, Sweden, 2004, pp. 26–30.
2 M. Armani, S. Chaudhary, R. Probst and B. Shapiro, in *18th IEEE International Conference on Micro Electro Mechanical Systems*, Miami, Florida, 2005, pp. 855–858.
3 M. Armani, S. Chaudhary, R. Probst and B. Shapiro, *J. Microelectromech. Syst.*, 2006, **15**, 945–956.
4 A. E. Cohen, *Phys. Rev. Lett.*, 2005, **94**, 118102.
5 A. E. Cohen and W. E. Moerner, *Appl. Phys. Lett.*, 2005, **86**, 093109–3.
6 C. Ropp, R. Jurgons, Z. Cummins, R. Kumar, A. J. Bergland, S. R. Raghavan, E. Waks and B. Shapiro, *Nano Lett.*, 2010, **10**, 2525–2530.
7 C. Ropp, Z. Cummins, S. Nah, J. T. Fourkas, B. Shapiro and E. Waks, *Nat. Commun.*, 2013, **4**, 1447.
8 D. P. J. Barz and P. Ehrhard, *Lab Chip*, 2005, **5**, 949–958.
9 J. G. Santiago, *Anal. Chem.*, 2001, **73**, 2353–2365.
10 D. J. Laser and J. G. Santiago, *J. Micromech. Microeng.*, 2004, **14**, R35.
11 R. Probst, *IEEE Control Syst. Mag.*, 2012, **32**, 26–53.
12 A. E. Cohen and W. E. Moerner, *Opt. Express*, 2008, **16**, 6941–6956.
13 C. Ropp, Z. Cummins, R. Probst, S. Qin, J. T. Fourkas, B. Shapiro and E. Waks, *Nano Lett.*, 2010, **10**, 4673–4679.
14 G. K. Batchelor, *An Introduction to Fluid Dynamics*, Cambridge University Press, 2000.
15 K. C. Neuman and S. M. Block, *Rev. Sci. Instrum.*, 2004, **75**, 2787–2809.
16 H. A. Pohl and H. A. Pohl, *Dielectrophoresis: the behavior of neutral matter in nonuniform electric fields*, Cambridge University Press, Cambridge, 1978, vol. 80.
17 R. E. Rosensweig, *Ferrohydrodynamics*, Courier Dover Publications, 1997.

18 P. P. Mathai, A. J. Berglund, J. A. Liddle and B. A. Shapiro, *New J. Phys.*, 2011, **13**, 013027.
19 P. P. Mathai, P. T. Carmichael, B. A. Shapiro and J. A. Liddle, *RSC Adv.*, 2013, **3**, 2677–2682.
20 J. King, M.S. Thesis, University of Tennessee, Knoxville, 2009.
21 L. Davis, Z. Sikorski, W. Robinson, G. Shen, X. Li, B. Canfield, I. Lescano, B. Bomar, W. Hofmeister, J. Germann, J. King, Y. White and A. Terekhov, in *Single-molecule spectroscopy and imaging*, ed. J. Enderlein, Proc. SPIE 6862, 2008, 68620P.
22 R. Probst and B. Shapiro, *J. Micromech. Microeng.*, 2011, **21**, 027004.
23 S. Chaudhary and B. Shapiro, *IEEE Trans. Control Syst.*, 2006, **14**, 669–680.
24 R. F. Probstein, *Physicochemical hydrodynamics: an introduction*, Wiley-Interscience, 2005.
25 R. P. Feynman, R. B. Leighton and M. L. Sands, *The Feynman Lectures on Physics: Mainly Electromagnetism and Matter*, Basic Books, 2011, vol. 2.
26 P. C. Hiemenz and R. Rajagopalan, *Principles of Colloid and Surface Chemistry, Third Edition,Revised and Expanded*, CRC Press, 1997.
27 C. E. Willert and M. Gharib, *Exp. Fluids*, 1992, **12**, 353–358.
28 M. Gharib, F. Pereira, D. Dabiri, J. R. Hove and D. Modarress, *Integr. Comp. Biol.*, 2002, **42**, 964–970.
29 L. Kajitani and D. Dabiri, *Meas. Sci. Technol.*, 2005, **16**, 790.
30 S. Y. Yoon and K. C. Kim, *Meas. Sci. Technol.*, 2006, **17**, 2897.
31 R. E. Kalman, *J. Basic Eng.*, 1960, **82**, 35–45.